Journal of Advanced Research 41 (2022) 145–158

Contents lists available at ScienceDirect

Journal of Advanced Research

journal homepage: www.elsevier.com/locate/jare

Original Article

Single-cell RNA sequencing analysis reveals the relationship of bone marrow and osteopenia in STZ-induced type 1 diabetic mice

Jinjie Zhong [a,2], Xingjia Mao [b,2], Heyangzi Li [c], Gerong Shen [d], Xi Cao [c], Ning He [d], Jingyu Wang [e], Lintao Xu [e], Jun Chen [a], Xinghui Song [f], Shuangshuang Liu [f], Xiaoming Zhang [c], Yueliang Shen [g], Lin-lin Wang [d,1], Chuan Xiang [b,1], Ying-ying Chen [a,*]

[a] Department of Basic Medicine Sciences, and Department of Obstetrics of the Second Affiliated Hospital, Zhejiang University School of Medicine, Hangzhou 310058, China
[b] Department of Orthopedic, The Second Hospital of Shanxi Medical University, Taiyuan 030001, China
[c] Department of Basic Medicine Sciences, and Department of Emergency Medicine, Sir Run Run Shaw Hospital, Zhejiang University School of Medicine, Hangzhou 310058, China
[d] Department of Basic Medicine Sciences, and Department of Orthopaedics of Sir Run Run Shaw Hospital, Zhejiang University School of Medicine, Hangzhou 310058, China
[e] Department of Neurosurgery, Second Affiliated Hospital of Zhejiang University School of Medicine, Hangzhou 310009, China
[f] Core Facilities, Zhejiang University School of Medicine, Hangzhou 310058, China
[g] Department of Basic Medicine Sciences, Zhejiang University School of Medicine, Hangzhou 310058, China

HIGHLIGHTS

- scRNA-seq analysis reveals the profiles of bone marrow cells in STZ-induced T1D mice.
- scRNA-seq analysis reveals the heterogeneity of bone marrow immune cells in STZ-induced T1D mice.
- The ratio of BM-neutrophils to B lymphocytes is increased in the bone marrow of STZ-induced T1D mice.
- Osteopenia is occurred in STZ-induced T1D mice.
- This increased ratio is negatively correlated with osteopenia in STZ-induced T1D mice.

GRAPHICAL ABSTRACT

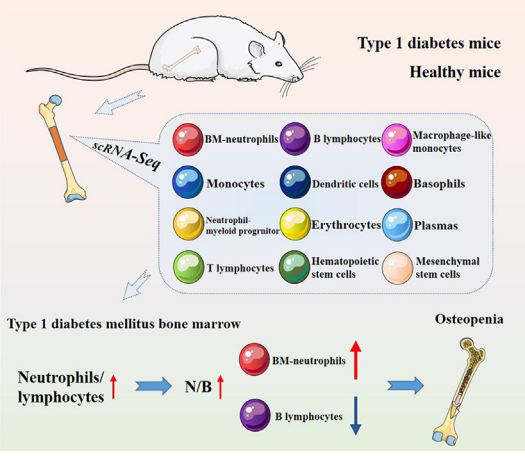

ARTICLE INFO

Article history:
Received 3 October 2021
Revised 30 November 2021
Accepted 14 January 2022
Available online 21 January 2022

Keywords:
Type 1 diabetes

ABSTRACT

Introduction: Type 1 diabetes (T1D) is a multifactorial autoimmune disease. Broad knowledge about the genetics, epidemiology and clinical management of T1D has been achieved, but understandings about the cell varieties in the bone marrow during T1D remain limited.
Objectives: We aimed to present a profile of the bone marrow cells and reveal the relationship of bone marrow and osteopenia in streptozotocin (STZ)-induced T1D mice.
Methods: The whole bone marrow cells from the femurs and tibias of healthy (group C) and STZ-induced T1D mice (group D) were collected for single-cell RNA sequencing analysis. Single-cell flow cytometry

Peer review under responsibility of Cairo University.
* Corresponding author.
E-mail addresses: wanglinlin@zju.edu.cn (L.-l. Wang), chuanxiang@sxmu.edu.cn (C. Xiang), bchenyy@zju.edu.cn (Y.-y. Chen).
[1] Co-corresponding authors.
[2] Jinjie Zhong and Xingjia Mao contributed equally to this work.

https://doi.org/10.1016/j.jare.2022.01.006

Single-cell RNA sequencing
Bone marrow
Osteopenia
Neutrophil
Lymphocyte

and immunohistochemistry were performed to confirm the proportional changes among bone marrow neutrophils (BM-neutrophils) ($Cxcr2^+$, $Ly6g^+$) and B lymphocytes ($Cd19^+$). X-ray and micro-CT were performed to detect bone mineral density. The correlation between the ratio of BM-neutrophils/B lymphocytes and osteopenia in STZ-induced T1D mice was analyzed by nonparametric Spearman correlation analysis.

Results: The bone marrow cells in groups C and D were divided into 12 clusters, and 249 differentially expressed genes were found. The diversity of $CD45^+$ immune cells between groups C and D were greatly affected: the proportion of BM-neutrophils showed a significant increase while the proportion of B lymphocytes in group D showed a significant decrease. X-ray and micro-CT analyses confirmed that osteopenia occurred in group D mice. In addition, the results of single-cell flow cytometry and correlation analysis showed that the ratio of BM-neutrophils/B lymphocytes negatively correlated with osteopenia in STZ-induced T1D mice.

Conclusion: A single-cell RNA sequencing analysis revealed the profile and heterogeneity of bone marrow immune cells in STZ-induced T1D mice for the first time. The ratio of BM-neutrophils/B lymphocytes negatively correlated with osteopenia in STZ-induced T1D mice, which may enhance understanding for treating T1D and preventing T1D-induced osteopenia.

Introduction

Type 1 diabetes (T1D) is characterized by chronic insulin deficiency and resultant hyperglycemia developed due to an autoimmune attack on pancreatic β cells [1,2]. The peak incidence of T1D onset is between 0 and 14 years old [3], but symptomatic onset has no age limitations [1]. Due to TID's severe symptoms and complications, increasing attention has been paid to its pathogenesis and related complication prevention. Increasing evidence has confirmed that T1D is associated with inflammation, and immune cells, such as neutrophils, macrophages, dendritic cells, and B lymphocytes, can initiate the diabetogenic T cell response and promote T1D [4]. In addition, changes in peripheral immune cell proportions are involved in aortic stiffness, a complication caused by T1D [5]. Moreover, T1D is complicated with mild to modest deficits in osteopenia and even osteopenic fracture [6–8]. However, there exists no definitive understanding of T1D-induced osteopenia's mechanism nor standard guidelines for its prevention. Therefore, there is an urgent need to better reveal the mechanism of T1D-induced osteopenia to reduce the risk of fractures, eventually hoping to improve the quality of life of T1D patients.

Neutrophils and lymphocytes are indispensable participants involved in various immune responses, and their levels are readily available through routine blood count analyses [5]. In addition, the neutrophil-to-lymphocyte ratio (NLR), with its simple, non-invasive, and cost-effective characteristics, has been widely available as a marker for inflammation and diseases, including cancer [9–11], coronavirus pneumonia 2019 (COVID-19)[12], and acute coronary syndrome [13]. A multisite longitudinal cohort study showed that high bone mineral density (BMD) loss was associated with an increased NLR [14,15]. Furthermore, patients with T1D were confirmed to have significantly higher peripheral NLR [5], implying that an increased NLR in peripheral blood is closely associated with osteopenia and T1D.

Bone marrow, thymus, and lymphoid tissues are dedicated immune system organs for immune cell development [16]. The most important is bone marrow, serving as the initial organ that produces immune cells. However, the changes in immune cells in the bone marrow of T1D patients are still unclear. Despite our knowledge about osteopenia [17,18] and increased NLR [5] in T1D patients and in peripheral blood, a hitherto unacknowledged role for NLR in the bone marrow during T1D has not yet been revealed.

In this study, using single-cell RNA sequencing technology, we revealed the profile and characteristics of whole bone marrow cells in STZ-induced T1D mice and discovered changes in the proportions of immune cells. BM-neutrophils and B lymphocytes with the most significant changes in proportion were focused on, and analyses were performed to dissect their pathogenic roles in STZ-induced T1D. We also explored the correlation between immune cells in the bone marrow and osteopenia in STZ-induced T1D mice. Thus, our study provides novel insights into STZ-induced T1D and osteopenia in STZ-induced T1D mice.

Materials and methods

Diabetes model

All experiments referring to animals were conducted in accordance with the guidelines of the Institutional Animal Care and Use Committee and approved by the Ethics Committee of Zhejiang University (Approval No. ZJU20210191). C57/BL6 mice (22–24 g, 8 weeks, male) were purchased from the Animal Center of Zhejiang University. Mice were maintained in cages (23 °C) on a 12-h light/-dark cycle with ad libitum access to food and water. All applicable international, national, and institutional guidelines for the care and use of animals were followed. The mice in the diabetes group were intraperitoneally injected with streptozotocin (STZ, 150 mg/kg, Sigma) to create type 1 diabetes models [21]. A high-dose injection with the genotoxic methylating agent STZ is one of the most common methods for establishing T1D rodent models since STZ rapidly destroys pancreatic β cells and results in typical T1D symptoms [19,20]. The mice in the sham group were injected with the same volume of sodium citrate solution. The blood glucose level of all mice was measured after 3 days to test for model establishment (blood glucose > 16.7 mmol/L). The mice were then fed with a regular diet, and their blood glucose level and weight were measured at 22 weeks and 28 weeks of age.

Bone marrow from three mice in each group aged 22 weeks was harvested from the femur and tibia, partly used for single-cell sequencing, and partly used for immunohistochemistry. The left femurs and tibias of six mice in group C (28 weeks) and five mice in group D (28 weeks) were used for X-ray and micro-CT. In addition, the four right legs from each group were dissected for flow cytometry analysis.

Bone marrow dissociation and preparation

After the mice were anesthetized with isoflurane [22], the heart was perfused with precooled PBS buffer (HyClone), and the femur and tibia were dissected. After removing the muscle and perios-

teum on the outer surfaces of the femur and tibia, three femurs and tibias of group C were combined into one sequencing sample and three femurs and tibias of group D were combined into one sequencing sample. The bones were cut into approximately 1 mm long fragments and digested with 1 mg/ml collagenase I/dispase II (Roche, 46793022). After incubating for 40 min at 37 °C, the cell suspension was filtered through a 40-μm cell strainer (Corning, 431751) to obtain a single-cell suspension and centrifuged at 1500*g* for 5 min [23]. Next, we resuspended the cells in 1x RBC lysis buffer (BioLegend, 420301) on ice for 5 min to remove the red blood cells. The solution was then centrifuged at 500*g* for 5 min and resuspended in PBS. Finally, the sample was stained with trypan blue (Sigma), and cell survival was evaluated microscopically.

Single-cell RNA sequencing

Single-cell suspensions were prepared at a concentration of 1×10^5 cells/mL in PBS then loaded onto microfluidic devices, where scRNA-seq libraries were constructed according to the Singleron GEXSCOPE® protocol by the GEXSCOPE® Single-Cell RNA Library Kit (Singleron Biotechnologies) [24]. Individual libraries were diluted to 4 nM and pooled for sequencing. Pools were sequenced on an Illumina HiSeq X with 150 bp paired-end reads.

scRNA-seq quantifications and statistical analysis

Raw reads were processed to generate gene expression profiles using an internal pipeline. Briefly, after filtering out read one without poly T tails, the cell barcode and unique molecular identifier (UMI) were extracted. Adapters and poly A tails were trimmed (fastp V1) before aligning read two to GRCh38 with ensemble version 92 gene annotation (fastp 2.5.3a and featureCounts 1.6.2) [25]. Reads with the same cell barcode, UMI, and gene were grouped to calculate the number of UMIs per gene per cell. Each cellular barcode's UMI count table was stored for further analysis. Cell type identification and clustering analysis were performed using the Seurat program [26,27] (http://satijalab.org/seurat/, R package, v.3.0.1), which was also applied for the RNA sequencing data analysis. UMI count tables were loaded into R using the read.table function. Then, we set the parameter resolution to 0.6 for the FindClusters function for clustering analyses. Next, differentially expressed genes (DEGs) between different samples or consecutive clusters were identified with the function FindMarkers. In addition, Gene Ontology (GO) function enrichment analysis and Kyoto Encyclopedia of Genes and Genomes (KEGG) pathway analysis were performed on the gene set using clusterProfiler software to identify biological functions or pathways that were significantly associated with the specific genes expressed [28].

RNA isolation and quantitative real-time PCR

Total RNA was extracted from the bone marrow form healthy and STZ-induced T1D mice with TRIzol reagent (Takara, China) according to the manufacturer's instructions. For mRNAs quantification, and reversely transcribed into cDNAs with the PrimeScript RT reagent Kit (Takara, China). The resulting cDNAs were quantified with SYBR Green reagent (Takara, China) by using the LightCycler 480II (Roche, Germany). The relative expression levels and quantification of mRNAs (Asprv1, Pim1, H1f0, Prok2, H2-Aa, H2-Eb1, Vpreb3 and Akap12) were calculated with the $2^{-\triangle\triangle Ct}$ method. Beta-actin was used as an internal control. All the primers were provided by Sunya (Zhejiang, China) listed in Table S2.

Immunohistochemistry

The femurs from the two groups at aged 22 weeks were fixed in 4% paraformaldehyde for 24 h. Then, the femur sections (5 μm) were decalcified, dehydrated, and paraffin-embedded using standard histologic techniques. Endogenous peroxidases were blocked with 3% H_2O_2. Next, antigen retrieval was completed with a complex digestive solution (AR0022; Boster), blocked with goat serum (AR0009; Boster), and then stained with CXCR2 (1:500; PAB18401; Abnova) and CD79a (1:500; RAB00679; Abnova) at 4 °C overnight. The sections were incubated with enhanced enzyme-labeled goat anti-rabbit IgG polymer (PV-9001; ZSGB-BIO), and the color reaction was conducted using DAB (ZLI-9018; ZSGB-BIO). The sections were scanned by a slide scanner using specific software (3DHISTECH, Ltd. Budapest, Hungary). The experiment was repeated more than three times.

Flow cytometry analysis

For single-cell flow cytometry, a single-cell suspension of bone marrow was collected as described in single-cell RNA sequencing [23]. After lysing and removing the red blood cells, we washed and resuspended the samples in staining buffer (BioLegend, 420201). Then, the samples were incubated with Fc block (BioLegend, 101302) for 10 min on ice to reduce non-specific immunofluorescent staining. For cell surface marker detection (CD45, Cxcr2, Ly-6g, CD19), cells were resuspended in 100 μl staining buffer, stained with primary antibody against surface markers for 30 min at 4 °C in the dark, and washed two times with staining buffer. For intracellular staining (Ki67), the cell pellet was resuspended in 250 μl Fix/Perm solution for 20 min at 4 °C, then washed twice in 1 × BD Perm/Wash buffer (BD Bioscience, 554714). Cells were then stained for intracellular molecules for 30 min at 4 °C in the dark and washed twice with 1 × BD Perm/Wash buffer. Finally, cell pellets were resuspended in staining buffer for flow cytometric analysis (Cytoflex Lx, Beckman Coulter), where gates and compensations were set before every experiment. All the antibodies mentioned above are listed in Table S1. The experiment was repeated more than three times.

Radiography

X-ray radiography was performed using a small-animal X-ray apparatus (UltraFocus, Faxitron) to detect the difference in BMD changes in group C(n = 6) and D(n = 5) mice's left legs. The exposure time and kV were set to the auto setting [29]. The window level was set from 2058 to 7200.

Computed tomography

Computed tomographic images of the left femurs in groups C (n = 6) and D (n = 5) were acquired using a micro-CT scanner (VivaCT80, SCANCO Medical Company, Switzerland) at high resolution. After the femur was reconstructed, BMD (mg HA/ccm), trabecular bone volume/total volume (BV/TV, %), trabecular thickness (Tb.Th, mm), trabecular number (Tb.N, 1/mm), and trabecular space (Tb.Sp, mm) [30] were assessed by scanner software (μCT Evaluation Program V6.5–3).

Statistical analysis

The data were presented as the means ± SEM and were statistically analyzed using GraphPad Prism (version 9.0; GraphPad Software, LCC). Student's t-tests were used when comparing two groups of data. Nonparametric Spearman correlation analysis was

used for correlation analyses. *P* values < 0.05 were considered to be significant.

Results

Profiles of bone marrow cells in healthy and STZ-induced T1D mice

We collected the whole bone marrow cells from the femurs and tibias of healthy (group C) and STZ-induced T1D mice (group D). After digestion and erythrolysis, 12,279 cells from group C and 15,118 cells from group D were collected for single-cell RNA-seq analysis (Fig. 1A). Fig. 1B demonstrated the unbiased clustering of all cells in group C and group D, originating from their co-analysis. The result revealed 12 cell clusters: spanning neutrophils (mainly expressing Cxcr2, Ly6g, and Ltf), monocytes (mainly expressing Fn1, Ccr2, and F13a1), neutrophil-myeloid progenitor (NMP, mainly expressing Elane, Mpo, and Prtn3), T lymphocytes (mainly expressing Cd3d, Ccl5, and Ms4a4b), B lymphocytes (mainly expressing Cd79a, Cd19, and Ighm), dendritic cells (DCs, mainly expressing Siglech, Irf8, and Bst2), erythrocytes (mainly expressing Hba-a1, Hbb-bs, and Hbb-bt), hematopoietic stem cell (HSC, mainly expressing Cd34, Adgrg1, and Cdk6), macrophages (mainly expressing C1qa, Vcam1, and Mrc1), basophils (mainly expressing Cd200r3, Mcpt8, and Prss34), plasma cells (mainly expressing Jchain, Iglc2, and Mzb1), and mesenchymal stem cells (MSC, mainly expressing Cxcl12, Col1a2, and Lepr) (Fig. 1C, D, G, H).

The proportional changes of different cell clusters in the bone marrow were discussed here. CD45, known as the common leukocyte antigen, is expressed by all immune cells. $CD45^+$ immune cells accounted for 95.44% of cells in group C and 96.33% of cells in group D (Fig. 1F); This result was consistent with that from the flow cytometry for CD45 in group C and group D (Fig. S1). In addition, these following cell clusters presented an increase in their proportion: BM-neutrophils increased from 46.94% to 64.04%; NMP increased from 3.47% to 6.48%; plasmas and T lymphocytes increased slightly. On the other hand, these following cell clusters presented a decrease in their proportion: B lymphocytes decreased sharply from 18.12% to 3.34%; DCs decreased significantly from 4.00% to 0.58%; macrophages, basophils, and monocytes decreased slightly. Among all immune cells mentioned above, the BM-neutrophils cell cluster had the most significant proportional increase, while the B lymphocytes cell cluster experienced the most significant proportional decrease the most (Fig. 1E, F).

There were 249 DEGs between groups C and D, including 69 upregulated and 180 downregulated genes. The top 20 most highly upregulated and downregulated DEGs are shown in Fig. S2. Besides, to confirm the results of single-cell RNA sequencing, the relative expression levels of eight DEGs selected randomly between groups C and D were validated by quantitative real-time PCR (Fig. S3). The results showed that there was the same DEGs expression trend between single-cell RNA sequencing and quantitative real-time PCR. GO enrichment analysis and KEGG pathway analysis were performed on the upregulated and downregulated DEGs. The most highly enriched biological process (BP), cellular component (CC), and molecular function (MF) terms among the upregulated DEGs were the response to interleukin-1, secretory granule, and antioxidant activity, respectively (Fig. S4). Conversely, the most enriched BP, CC, and MF terms among the downregulated DEGs were cytoplasmic translation, cytosolic ribosome, and structural constituent of ribosome, respectively (Fig. S6). In addition, the most enriched pathways among the upregulated DEGs were IL-17 signaling pathway, AGE-RAGE signaling pathway in diabetic complications, TNF signaling pathway, and osteoclast differentiation (Fig. S5). In contrast, the most enriched pathways among the downregulated DEGs were those associated with ribosome, antigen processing and presentation, and B cell receptor signaling pathway (Fig. S7).

Heterogeneity of BM-neutrophils in the bone marrow of STZ-induced T1D mice

As previously mentioned, BM-neutrophils presented the largest proportional increase among all the immune cells in group D. To explore the heterogeneity of BM-neutrophils, we analyzed the characteristics of the BM-neutrophil subsets. The results showed that the BM-neutrophils could be subdivided into 6 subsets (Fig. 2A–C): BM-neutrophil_1 (mainly expressing Asprv1, Prok2, and Fbxl5), BM-neutrophil_2 (mainly expressing Ltf, Zmpste24, and Cybb), BM-neutrophil_3 (mainly expressing Clec4d, Thbs1, and Egr1), BM-neutrophil_4 (mainly expressing Ube2c, Mki67, and Top2a), BM-neutrophil_5 (mainly expressing Pcna, Rrm2, and Pclaf), and BM-neutrophil_6 (mainly expressing Actb, CT010467.1, and Tmsb4x) (Fig. 2B, F). The proportional changes of each subset were as the following: BM-neutrophil_1 increased the most, spiking from 5.97% to 50.14%; BM-neutrophil_2 decreased from 34.4% to 19.12%; BM-neutrophil_3 decreased from 38.53% to 3.13%; BM-neutrophil_4 decreased from 16.22% to 15.33%; BM-neutrophil_5 increased slightly from 4.2% to 5.67%; BM-neutrophil_6 increased slightly from 0.68% to 6.61%. Compared with group C, the proportion of BM-neutrophil_1 demonstrated an impressive increase. Conversely, the proportion of BM-neutrophil_3 presented a most significant decrease (Fig. 2D). Moreover, we performed immunohistochemistry staining to validate the increase in BM-neutrophils (marked by CXCR2) in group D (Fig. 2E).

Among all DEGs in the 6 neutrophil subsets, Asprv1, Ltf, Clec4d, Ube2c, Pcna, and Actb were DEGs with the most significant changes in proportion. Asprv1, a mammalian retroviral-like enzyme [31], and Clec4d, a trehalose-6,6′-dimycolate receptor [32], were both expressed in the BM-neutrophil_1 and BM-neutrophil_3 subsets (Fig. 2E). Asprv1 and Clec4d showed the most significant changes among BM-neutrophil_1 and BM-neutrophil_3, respectively. Ltf, an extracellular iron-binding glycoprotein [33], and Actb, were both expressed in whole bone marrow cells and the 6 BM-neutrophil subsets (Fig. 2E). Ube2c, a member of the ubiquitin modification system [34], and Pcna, a gene associated with cell proliferation, were mainly expressed in BM-neutrophil_4 and BM-neutrophil_5, respectively (Fig. 2F).

Next, pseudotime analysis of the 6 subsets of BM-neutrophils was carried out using Monocle. The results suggested that there were two diverging cell fates, one starting with BM-neutrophil_4 and BM-neutrophil_5 and differentiating towards BM-neutrophil_1 or BM-neutrophil_3, and the other starting with BM-neutrophil_2 and BM-neutrophil_6 and differentiating towards BM-neutrophil_1 or BM-neutrophil_3 (Fig. 3A–D). Moreover, the ordering was captured by latent time and RNA velocity (Fig. 3E).

Furthermore, because BM-neutrophil_1 made up the highest proportion of cells in group D, GO enrichment analysis and KEGG pathway analysis were performed for the upregulated DEGs in BM-neutrophil_1. The results showed that most of the biological processes enriched among the DEGs in BM-neutrophil_1 were related to the hexose metabolic process, another glucose metabolism, anabolism, and cytokine–mediated signaling pathway. Extracellular vesicles, including exosomes and other organelles, were the most common cellular components (Fig. 3G). KEGG pathway analysis indicated that osteoclast differentiation, IL-17 signaling pathway, and TNF signaling pathway were the most highly enriched pathways among the DEGs (Fig. 3H). As listed in Fig. 3I–J, the top 5 most upregulated DEGs were Asprv1, Pim1, Cebpb,

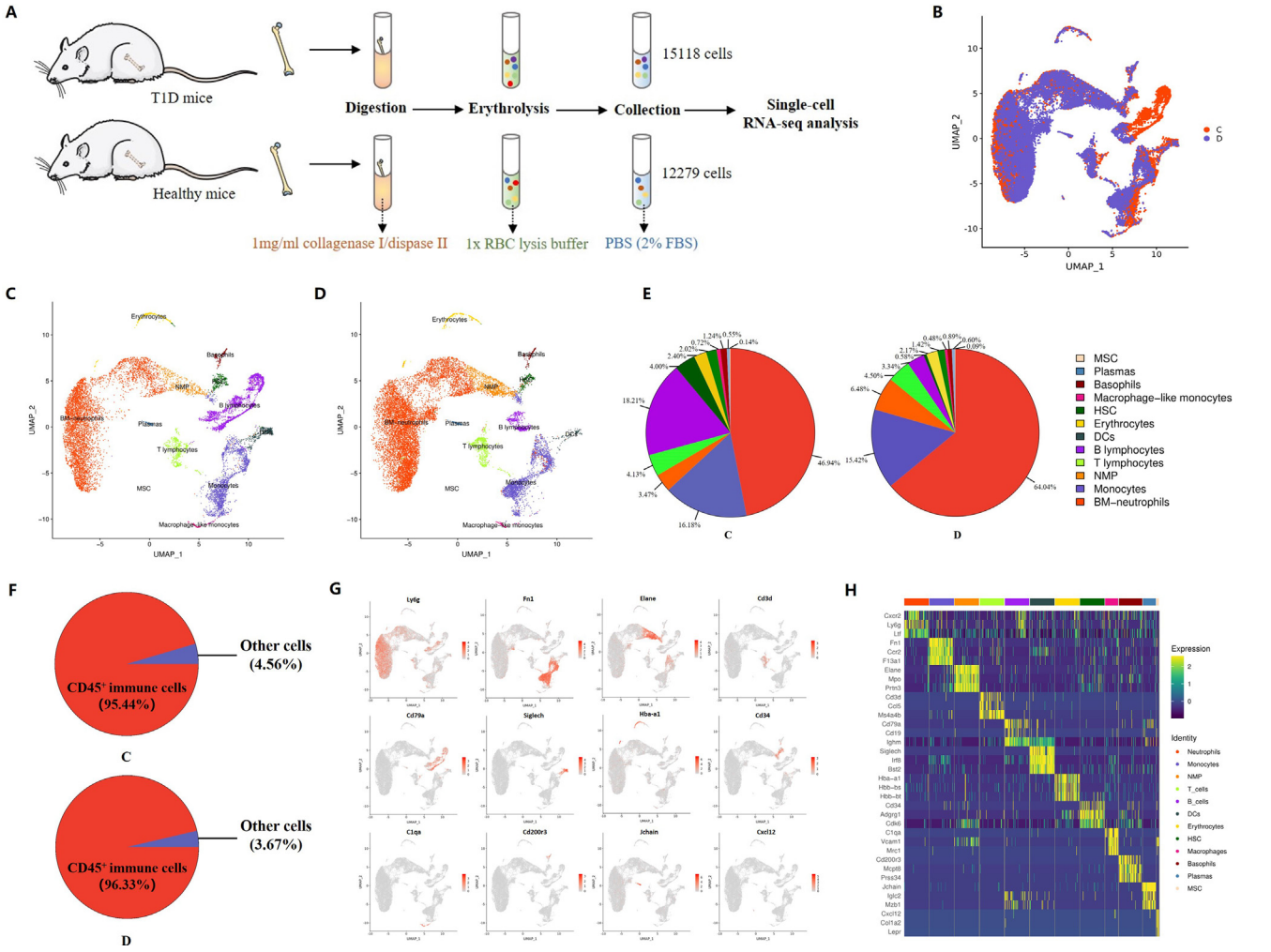

Fig. 1. A single-cell RNA sequencing revealed the atlas of bone marrow cells in healthy and STZ-induced T1D mice. (A) Study overview. (B-D) Twelve bone marrow cells clusters. UMAP of unbiased clustering of all bone marrow cells in groups C and D (B). UMAP of unbiased clustering and cell annotation of bone marrow cells in group C (C). UMAP of unbiased clustering and cell annotation of bone marrow cells in group D (D). (E) The proportions of each cell in groups C and D. (F) The specific proportion of $CD45^+$ cells in groups C and D. (G) Key cell type marker genes of 12 cell clusters, the redder the color, the higher the expression. (H) Cluster signature genes highlighted on left. Expression of top differentially expressed genes (rows) across the cells (columns), the warmer the color, the higher the expression.

H1f0, and Prok2, and the top 5 most downregulated DEGs were Lyz2, Ifitm3, Thbs1, S100a8, and Lcn2. We mixed bone marrow cells from three mice into one sequencing sample in group C or in group D. The biological duplication was achieved. But as for single-cell sequencing sample analysis, the sample number is only one, so histograms in Fig. 3 did not present statistical analysis.

Heterogeneity of B lymphocytes in the bone marrow of STZ-induced T1D mice

We next examined the characteristics and differentiation of B lymphocytes. Common marker genes to annotate B lymphocytes are Bank1 [35], CD83 [36], and Ighd [37] (Fig. 4F). The top 5 most upregulated genes were H2-Aa, Ighd, Macf1, Ptpn22, and H2-Eb1. The top 5 most downregulated genes were Vpreb3, Top2a, Mki67, Akap12, and Myb. Both sets of DEGs were shown in Fig. 4J and K. Because the sample number was one in each group for single-cell sequencing sample analysis, so the histograms in Fig. 4 did not present statistical analysis. B lymphocytes could be separated into two subsets, precursor B cells (Pre_B), and Naïve_B cells (Naïve_B). Their unbiased clustering was shown in Fig. 4A–C. We observed that the Pre_B group was the dominant subset in group C, while only the Naïve_B subset was present in group D (Fig. 4D). Immunohistochemistry validated that the number of B lymphocytes (marked by CD79a) were decreased in group D (Fig. 4E). In addition, latent time and RNA velocity analysis showed that the Pre_B subset was produced earlier than the Naïve_B subset (Fig. 4G).

GO enrichment analysis and KEGG pathway analysis were performed for the upregulated DEGs in B cells. GO enrichment analysis showed that most of the enriched biological processes were associated with antigen processing and presentation of peptide antigen via MHC class II, antigen processing and presentation of peptide or polysaccharide antigen via MHC class II, and lymphocyte proliferation. Enriched cellular components mainly included the MHC protein complex, late endosome, and lysosome. MHC protein complex binding was the major molecular function (Fig. 4H). KEGG pathway analysis indicated that DEGs were mainly enriched for immune-related diseases, including tuberculosis and asthma, antigen processing and presentation, and hematopoietic cell lineage (Fig. 4I).

Heterogeneity of monocytes, T lymphocytes, and DCs in the bone marrow of STZ-induced T1D mice

We analyzed monocytes, T lymphocytes, and DCs, respectively. The changes in the proportion of each subset were analyzed and shown in Fig. 5.

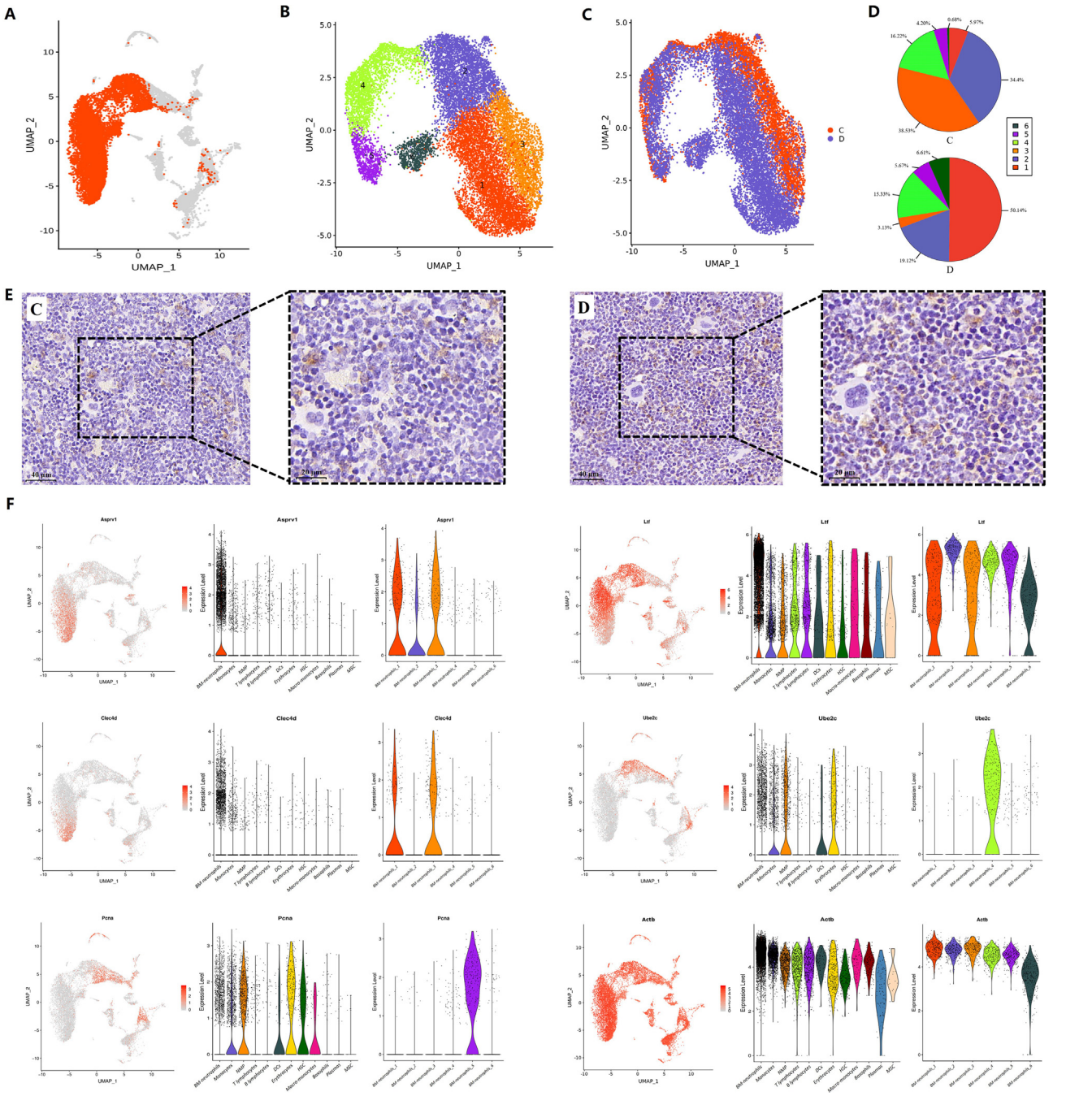

Fig. 2. The characteristics of BM-neutrophils between groups C and D. (A) UMAP of BM-neutrophil cluster among all cells. (B-C) Six BM-neutrophil subsets. UMAP of unbiased clustering and cell annotation of BM-neutrophil subsets in groups C and D (B). UMAP of unbiased clustering of BM-neutrophil subsets in groups C and D (C). (D) The proportion of BM-neutrophil subsets in groups C and D. (E) BM-neutrophils were labeled by immunohistochemistry of the sections of femur in groups C and D (CXCR2; Scale bar, 40 μm or 20 μm) (F) Key marker genes of BM-neutrophil subsets. UMAP of key marker genes of BM-neutrophil subsets, along with the corresponding distribution of expression levels among 12 clusters and 6 BM-neutrophil subsets respectively. Key marker genes included Asprv1, Ltf, Clec4d, Ube2c, Pcna and Actb.

Monocytes were subdivided into 5 subsets, including classical monocytes (mainly expressing Fn1, Tmsb10, and Crip1), neutrophils (mainly expressing Retnlg, Ngp, and Camp), NMP (mainly expressing Mpo, Prtn3, and Ncl), nonclassical monocytes (mainly expressing Ace, Cd36, and Apoe) and macrophages (mainly expressing Cd74, H2-Aa, and H2-Ab1) (Fig. 5A, D). The unbiased clusters of these subsets were shown in Fig. 5A–B. The proportional changes of each subset were as follows: classical monocytes decreased from 71.09% to 60.75%; neutrophils increased from 15.39% to 27.85%; NMP increased from 5.46% to 7.66%; classical nonclassical monocytes increased slightly from 2.91% to 3.48%; macrophages decreased from 5.15% to 0.26%. Except for the macrophage subset that decreased noticeably, the proportions of the other subsets experienced no obvious changes compared to group C (Fig. 5C).

T lymphocytes play a critical role in the pathogenesis of T1D [38,39]. Therefore, we next analyzed the profile of T lymphocytes in the bone marrow of STZ-induced T1D mice. The T lymphocytes were divided into 4 subsets, including natural killer T cells (NKT, expressing Ly6c2, Ccl5, and Cd69), naïve T cells/central memory T cells (Naïve T cells or Tcm, mainly expressing Ccr7, Hbb-bs, and Gm14085), natural killer cells (NK, mainly expressing Gzma, Klra8,

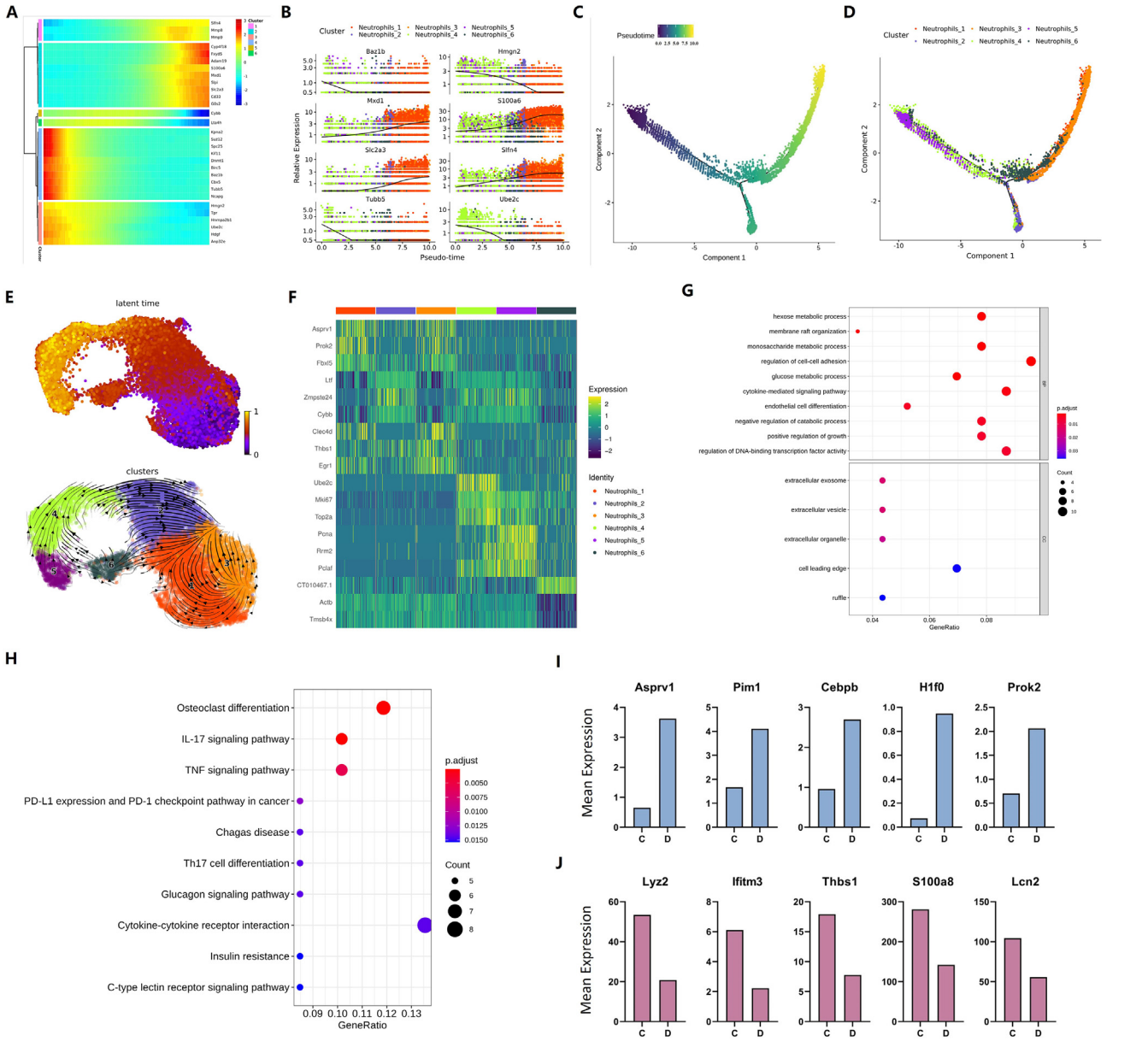

Fig. 3. Differential trajectory of BM-neutrophil subsets and enrichment of DEGs. (A-D) Differential directions of 6 BM-neutrophil subsets. Heatmap presenting relative expressions of markers of BM-neutrophils along inferred trajectories in 6 BM-neutrophil subsets. The red and blue branches correspond to the two differential directions (A). Monocle pseudotime trajectory expression pattern of 6 BM-neutrophil subsets (B). Pseudotime trajectories of the BM-neutrophil subsets (C-D). (E) Latent time and RNA velocity of 6 BM-neutrophil subsets. Latent time and RNA velocity showed the internal clock of BM-neutrophil subsets. Different colors of latent time represent different differentiation times, the colder the color, the earlier, the warmer the color, the later; The arrows of RNA velocity represent the different directions of differentiation. (F) Signature genes of BM-neutrophil subsets. Subset signature genes highlighted on left. Expression of signature genes (rows) across the cells (columns), the warmer the color, the higher the expression. (G) GO analysis of BM-neutrophil_1. Bubble diagram of upregulated DEGs of BM-neutrophil_1 enriched in GO analysis. (H) KEGG analysis of BM-neutrophil_1. Bubble diagram of upregulated DEGs of BM-neutrophil_1 enriched in KEGG analysis. (I-J) The top 5 DEGs of BM-neutrophils. The top 5 upregulated DEGs between groups C and D (I). The top 5 downregulated DEGs between groups C and D (J).

and Klra4), and CD4$^+$ T cells (CD4$^+$ T, mainly expressing Rora, Ikzf2, and Ttn) (Fig. 5E, H). The unbiased clusters of these subsets were shown in Fig. 5E–F. The proportional changes of each subset were as follows: NKT decreased from 49.32% to 36.0%; Naïve T cells or Tcm increased from 26.03% to 51.73%; NK decreased from 18.15% to 10.4%; CD4$^+$ T decreased from 6.51% to 1.87%. Except for the obvious increase in the proportion of Naïve T cells or Tcm, the other T lymphocytes subsets had a decreasing trend in proportion in group D(Fig. 5G).

DCs also experienced one of the most significant decreases in proportion among cells and were subdivided into 4 subsets, described as DCs_1 (mainly expressing Klk1, Cd74, and H2-Aa), DCs_2 (mainly expressing Stat1, Runx2, and Ly6d), DCs_3 (mainly expressing Top2, Mki67, and Hist1h1b) and DCs_4 (mainly expressing Prtn3, F13a1, and Mcm3) (Fig. 5I, L). The unbiased clustering of these subsets was shown in Fig. 5I–J. The proportional changes of each subset were as follows: DCs_1 decreased from 39.89% to 7.94%; DCs_2 increased from 26.59% to 39.68%; DCs_3 increased from 18.28% to 25.40%; DCs_4 increased from 15.24% to 26.98% (Fig. 5K). Except for the significant decrease in the proportion of DCs_1, the other DC subsets experienced slight increases in cell proportion in group D.

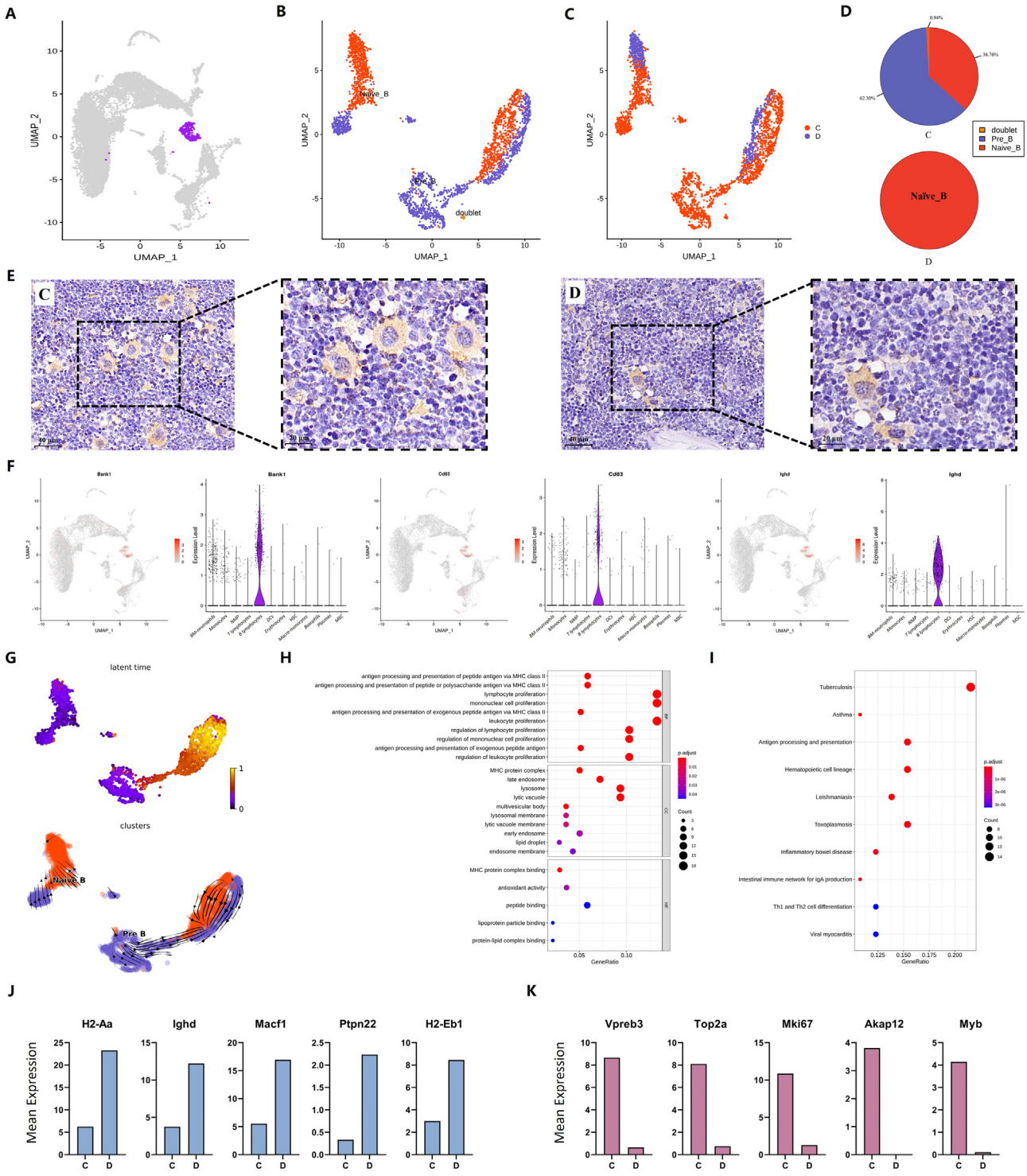

Fig. 4. The characteristics of B lymphocytes between groups C and D. (A) UMAP of the cluster of B lymphocytes among all cells. (B-C) Two B lymphocyte subsets. UMAP of unbiased clustering and cell annotation of the subsets of B lymphocytes in groups C and D (B). UMAP of unbiased clustering of the subsets of B lymphocytes in groups C and D (C). (D) The proportion of the subsets of B lymphocytes in groups C and D. (E) B lymphocytes were labeled by immunohistochemistry of the sections of femur in groups C and D (CD79a; Scale bar, 40 μm or 20 μm). (F) Key marker genes of B lymphocyte subsets. UMAP of key marker genes of the subsets of B lymphocytes, along with the corresponding distribution of expression levels among 12 clusters. Key marker genes included Bank1, CD83 and Ighd. (G) Latent time and RNA velocity of 3B lymphocyte subsets. Latent time and RNA velocity showed the internal clock of B lymphocyte subsets. Different colors of latent time represent different differentiation times, the colder the color, the earlier, the warmer the color, the later; The arrows of RNA velocity represent the different directions of differentiation. (H) GO analysis of Naïve_B. Bubble diagram of upregulated DEGs of Naïve_B enriched in GO analysis. (I) KEGG analysis of Naïve_B. Bubble diagram of upregulated DEGs of Naïve_B enriched in KEGG analysis. (J-K) The top 5 DEGs of B lymphocytes. The top 5 upregulated DEGs between groups C and D (J). The top 5 downregulated DEGs between groups C and D (K).

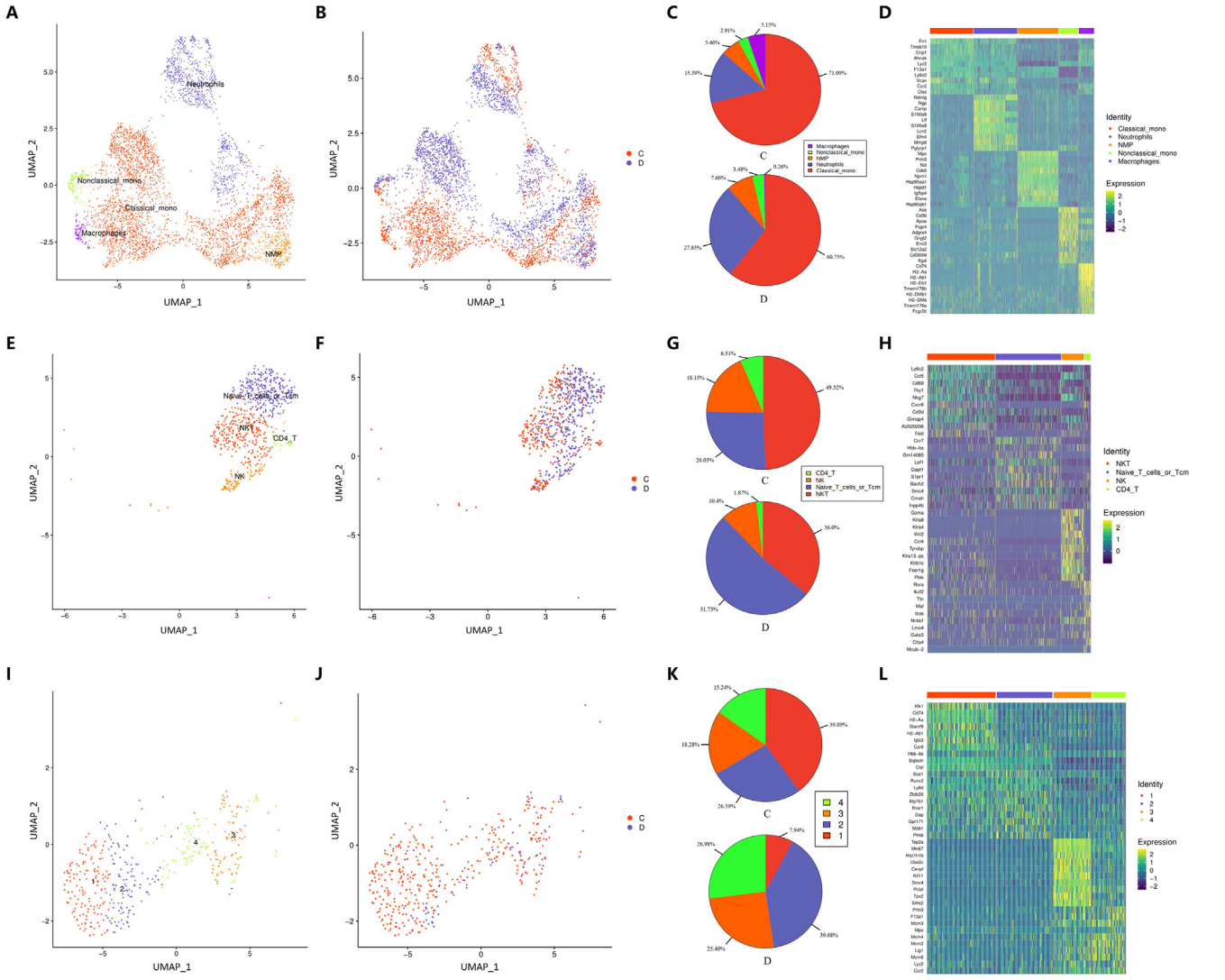

Fig. 5. The characteristics of monocytes, T lymphocytes and DCs between groups C and D. (A-B) Five monocyte subsets. UMAP of unbiased clustering and cell annotation of the subsets of monocytes in groups C and D (A). UMAP of unbiased clustering of the subsets of monocytes in groups C and D (B). (C) The proportion of the subsets of monocytes in groups C and D. (D) Signature genes of monocyte subsets. Subset signature genes highlighted on left. Expression of signature genes (rows) across the cells (columns), the warmer the color, the higher the expression. (E-F) Four T lymphocyte subsets. UMAP of unbiased clustering and cell annotation of the subsets of T lymphocytes in groups C and D (E). UMAP of unbiased clustering of the subsets of T lymphocytes in groups C and D (F). (G) The proportion of the subsets of T lymphocytes in groups C and D. (H) Signature genes of T lymphocyte subsets. Subset signature genes highlighted on left. Expression of signature genes (rows) across the cells (columns), the warmer the color, the higher the expression. (I-J) Four dendritic cell subsets. UMAP of unbiased clustering and cell annotation of the subsets of DCs in groups C and D (I). UMAP of unbiased clustering of the subsets of DCs in groups C and D (J). (K) The proportion of the subsets of DCs in groups C and D. (L) Signature genes of dendritic cell subsets. Subset signature genes highlighted on left. Expression of signature genes (rows) across the cells (columns), the warmer the color, the higher the expression.

Osteopenia in STZ-induced T1D mice

The weight and blood sugar levels of all groups of mice were measured at 22 W and 28 W of age. The results showed that our T1D model was successful (Fig. 7A). To identify whether osteopenia occurred in STZ-induced T1D mice, we used X-ray and micro-CT to analyze the changes in bone mass in groups C (28w, n = 6) and D (28w, n = 5). Fig. 6A showed the X-ray images of femurs and tibias, where it was clear that BMD had decreased in group D compared with group C. Moreover, the micro-CT images of the same part of the femur showed that the cortical bone was obviously thinner in group D. BMD ($P < 0.001$), trabecular bone volume/total volume (BV/TV) ($P < 0.001$), and trabecular thickness (Tb.Th) ($P < 0.001$) also experienced significant decreases in the femurs of group D (Fig. 6C). Meanwhile, trabecular number (Tb.N) ($P = 0.098$) and trabecular space (Tb.Sp) ($P = 0.085$) experienced decreased and increased trend, respectively (Fig. 6C). In summary, it was confirmed that osteopenia could occur in STZ-induced T1D mice.

Ratios of immune cells in the bone marrow of STZ-induced T1D mice

Increased NLR in the blood is correlated with bone loss and has been proposed as an index of related diseases, including osteoporosis in postmenopausal women and elderlies [15,40]. This critical correlation prompted us to explore if the change in NLR in peripheral blood originates from the change in ratios of immune cells in the bone marrow in T1D-induced osteopenia. Compared with group C, group D demonstrated an increased proportion of particular CD45$^+$ immune cells, mainly BM-neutrophils, monocytes (including macrophage-like monocytes), and T lymphocytes. Meanwhile, group D also demonstrated a decreased proportion of other particular CD45$^+$ immune cells, mainly B lymphocytes and DCs. The specific proportions of immune cells came from the

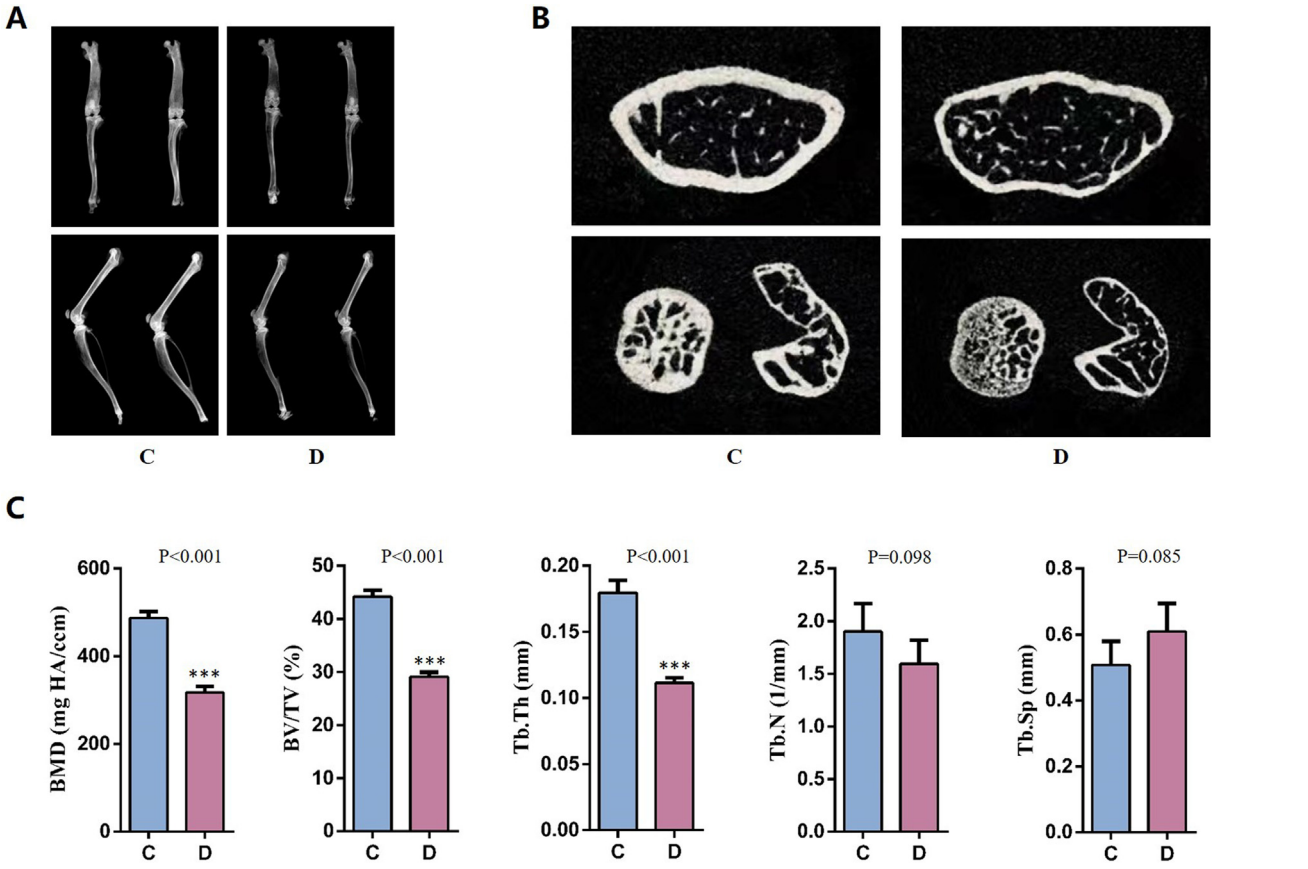

Fig. 6. Osteopenia occurred in STZ-induced T1D mice. (A) X-ray imaging of left legs in groups C and D. It can be seen intuitively that the BMD of group C was higher than that of Group D. Window level was set from 2058 to 7200. (B) Micro-CT imaging of the same part of femurs in groups C and D. It can be seen intuitively that the bone cortex of group C was thicker than that of group D. (C) Micro-CT analysis. The results showed BMD (***$p < 0.001$), BV/TV (***$p < 0.001$), Tb.Th (***$p < 0.001$), Tb.N ($p = 0.098$) and Tb.Sp ($p = 0.085$).

results of the single-cell RNA sequencing analysis. The ratios of the above immune cells between groups C and D are shown in Fig. 7B. RD/RC (the ratio of cells in group D/ cells in group C) was used to illustrate the differences in the ratios between groups C and D. We can see from Fig. 7C that the RD/RC of BM-neutrophil_1/Naïve_B was the highest. Moreover, there was an increasing trend in the RD/RC of BM-neutrophils/DCs, BM-neutrophils/B lymphocytes, monocytes/DCs, and monocytes/B lymphocytes. The above result found that the ratio of BM-neutrophils/B lymphocytes increased in bone marrow, similar to the increase of NLR in peripheral blood.

Ratio of BM-neutrophils and B lymphocytes in bone marrow was related to osteopenia in STZ-induced T1D mice

Next, we performed single-cell flow cytometry to validate the changes in proportion for BM-neutrophil ($Cxcr2^+$, $Ly6g^+$) [41,42] and B lymphocyte ($Cd19^+$) [43] in groups C (right, n = 4) and D (right, n = 4) (Fig. 8A). The ratio of BM-neutrophils/B lymphocytes ($P = 0.040$) was shown in Fig. 8B. We performed a correlation analysis (GraphPad Prism 9.0) between the ratio of BM-neutrophils/B lymphocytes and the ratio of BV/TV (corresponding left, n = 4). The results demonstrated that there was a negative correlation between the ratio of BM-neutrophils/B lymphocytes and the ratio of BV/TV (r = -0.7619, $P = 0.0368$) (Fig. 8C).

Discussion

T1D is largely portrayed as an autoimmune disease. However, research has yet given the role of the bone marrow, the initial organ producing immune cells, in T1D sufficient attention. To understand the varieties of bone marrow cells of T1D, we conducted a single-cell RNA sequencing analysis of whole bone marrow cells from the femurs and tibias of STZ-induced T1D mice for the first time. STZ-induced TID was used as the model since it has been considered a representative model of T1D [21]. The result presented an unbiased clustering of all cells, and we focused on the changes in immune cells in the bone marrow between healthy and STZ-induced T1D mice. Furthermore, the characteristics of BM-neutrophils, B lymphocytes, monocytes, T lymphocytes, and DCs were identified.

As a result of the increased incidence and prevalence of T1D, the number of patients at risk for T1D-induced osteopenia is expected to rise [6,44]. Thus, we also explored the relationship between immune cells in the bone marrow and osteopenia in STZ-induced T1D mice. We found that the proportion of BM-neutrophils increased most significantly, and the proportion of B lymphocytes decreased most significantly. The increased ratio of BM-neutrophils/B lymphocytes was negatively correlated with T1D-induced osteopenia. Our results revealed the profiles of bone marrow cells in STZ-induced T1D mice and the correlation between immune cells and osteopenia, which may contribute to a better understanding of the pathogenesis of STZ-induced T1D and osteopenia in STZ-induced T1D mice.

As universally acknowledged, bone marrow neutrophils (immature neutrophils) are usually divided into 5 subsets according to the morphology of the nucleus, including myeloblast, promyelocyte, myelocyte, metamyelocyte, and stab granulocyte. Our discovery could provide a new classification for BM-neutrophils,

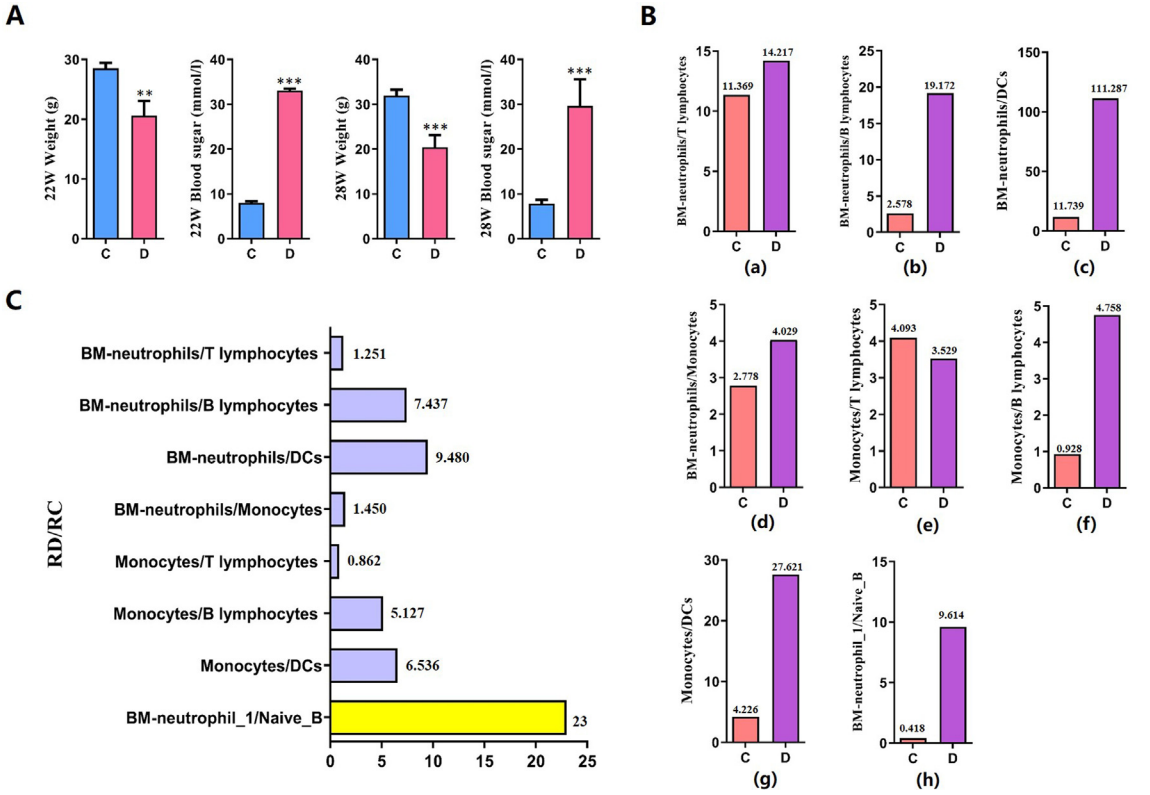

Fig. 7. Identification of STZ-induced T1D mice and the ratio of immune cells between groups C and D. (A) The weight and blood sugar between group C and D. The weight and blood sugar of STZ-induced T1D mice were detected at ages of 22 W and 28 W (**$p < 0.01$, ***$p < 0.001$). (B) The ratio of different immune cells. The ratio of BM-neutrophils/T lymphocytes, BM-neutrophils/B lymphocytes, BM-neutrophils/DCs, BM-neutrophils/monocytes, monocytes/T lymphocytes, monocytes/B lymphocytes, monocytes/DCs, BM-neutrophil_1/Naïve_B in groups C and D. (C) The RD/RC among different immune cells. The RD/RC of BM-neutrophils/T lymphocytes, BM-neutrophils/B lymphocytes, BM-neutrophils/DCs, BM-neutrophils/monocytes, monocytes/T lymphocytes, monocytes/B lymphocytes, monocytes/DCs, BM-neutrophil_1/Naïve_B.

subdividing them into 6 subsets according to their DEGs for the first time. We speculate that there may be an intersection among the two classifications of the BM-neutrophils subset. More importantly, the DEG-based classification may be more helpful for studying specific functions of neutrophil subsets. The proportion of BM-neutrophil_1 was highest, while the proportion of other subsets all tended to differentiate into BM-neutrophil_1. GO analysis of the upregulated DEGs between BM-neutrophil_1, and the other subsets indicated that extracellular vesicles, including exosomes and other organelles, were the most enriched cellular component term, consistent with the GO analysis of the upregulated DEGs between healthy and STZ-induced T1D mice.

KEGG pathway analysis of BM-neutrophil_1 indicated that it was mainly enriched for osteoclast differentiation, IL-17 signaling pathway, and TNF signaling pathway. This result was also consistent with the KEGG analysis of the upregulated DEGs between healthy and STZ-induced T1D mice. These results demonstrated that the BM-neutrophil_1 subset might be closely involved in the pathological processes of T1D and T1D-induced osteopenia. Furthermore, it has been confirmed that there is a reduction in circulating neutrophils in T1D patients [45–48]. Several explanations have been proposed for the decrease in circulating neutrophils, such as an impairment in neutrophil output from the bone marrow, the differentiation of neutrophils, an increase in peripheral consumption, destruction of neutrophils, or tissue sequestration [45]. However, the exact mechanisms responsible for the reduction in circulating neutrophils are still unclear. According to our results, flow cytometry of Ki67 showed no significant difference in cell proliferation (Fig. S8). Meanwhile, the proportion of neutrophils increased notably, suggesting that a limited neutrophil outflow from the bone marrow seems to be involved. However, this potential mechanism requires further in-depth study.

Additionally, evidence has shown that B lymphocytes also play a key role in the pathogenesis of T1D [43,49]. Among bone marrow cells, B lymphocytes experienced the most significant decrease in proportion. B lymphocytes could be subdivided into Pre_B and Naïve_B. Only Naïve_B was presented in STZ-induced T1D mice, and the enrichment analysis mainly reflected terms related to promoting the immune response by antigen processing and presentation. In addition, enhanced lymphocyte proliferation was highly expressed in the bone marrow of STZ-induced T1D mice, which is consistent with the critical role of B cells in the pathogenesis of T1D [49] and their therapeutic potential for T1D [43]. Other immune cells with significant proportional changes mainly included monocytes, T lymphocytes, and DCs. Excluding the proportion change of B lymphocytes, we found that DCs experienced the subsequent largest decrease in proportion. The increase in monocytes in STZ-induced T1D mice was mirrored by an increase in the neutrophil subset, which suggested that there may be a transformation of monocytes to neutrophils. The increase of the proportion of T cells in STZ-induced T1D mice mainly comprised an increase in Naïve T cells or Tcm. This increase in Naïve T cells could prevent chronic infection and control systemic secondary infections with their stem cell-like capacity to expand, differentiate, and self-renew [50].

Furthermore, the X-ray and micro-CT imaging analysis results showed a significant reduction in the BMD of STZ-induced T1D mice, consistent with previously published results [7]. We then determined the ratio between two sets of immune cells among BM-neutrophils (set monocytes and T lympho-

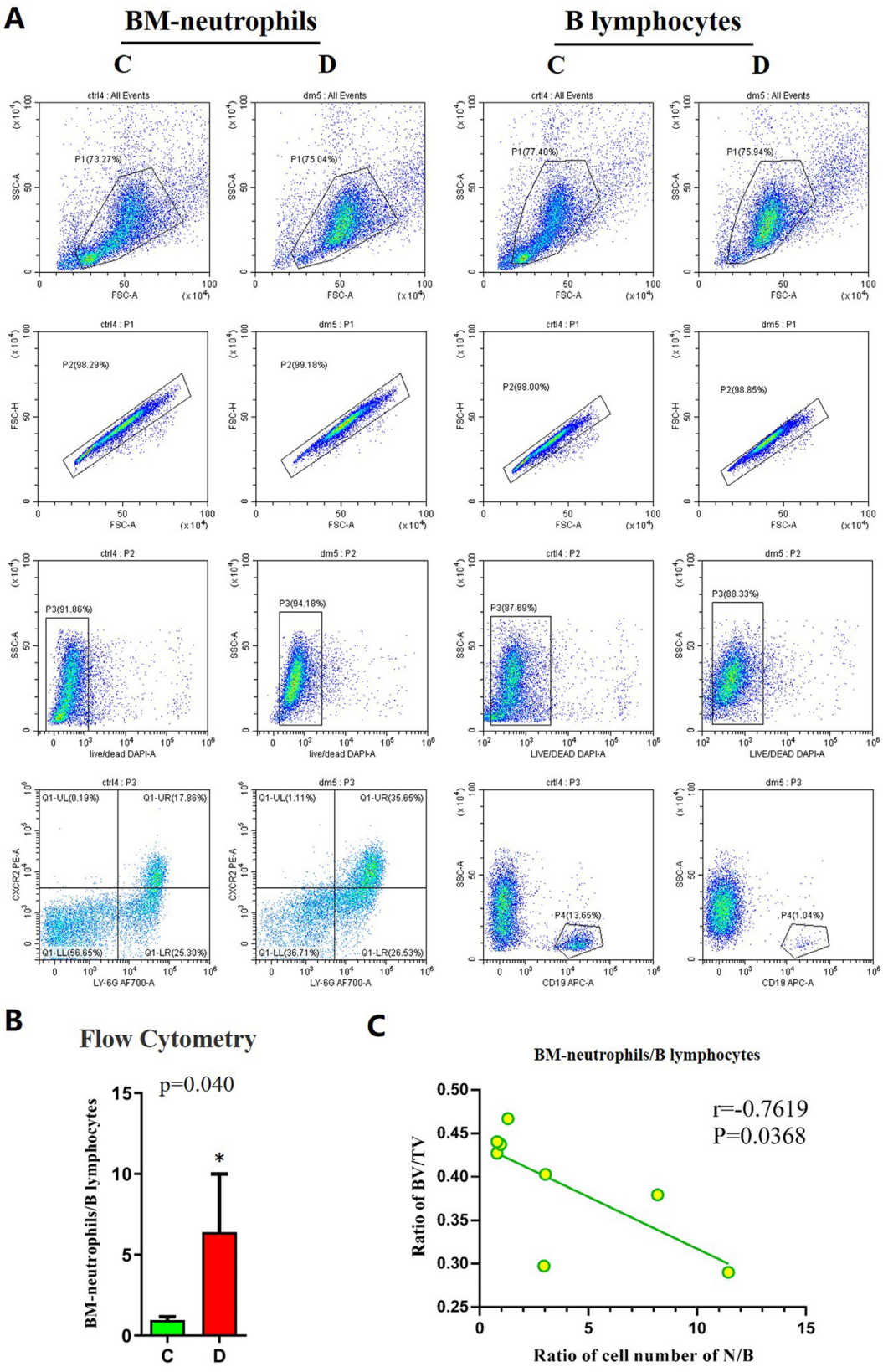

Fig. 8. The correlation between immune cells and osteopenia. (A) Flow cytometry of BM-neutrophils and B lymphocytes from bone marrow. The proportion of BM-neutrophils increased notably in group D and the proportion of B lymphocytes decreased notably in group D. (B) The ratios of BM-neutrophils/B lymphocytes from the results of flow cytometry. The ratio of BM-neutrophils/B lymphocytes was notably higher in group D (p = 0.040). (C) The correlation analysis between the ratio of BM-neutrophils/B lymphocytes and the ratio of BV/TV. There was a negative correlation between the ratio of BV/TV and the ratio of BM-neutrophils/B lymphocytes. (r = -0.7619, p = 0.0368). (*p < 0.05).

cytes and DCs) in healthy and STZ-induced T1D mice. The RD/RC of BM-neutrophils/B lymphocytes was increased in the bone marrow. Next, flow cytometry verified that the ratio of BM-neutrophils/B lymphocytes might be more meaningful between healthy and STZ-induced T1D mice. Moreover, as it is known that both osteopenia and increased NLR could occur in T1D patients [5,17,18], it is worth discussing whether the increased ratios of BM-neutrophils/B lymphocytes in the bone marrow was associated with osteopenia in STZ-induced T1D mice. We then conducted a correlation analysis, which indicated that there was a negative correlation between the ratio of BM-neutrophils/B lymphocytes and the ratio of BV/TV, consistent with increased peripheral NLR in T1D patients. Thus, we speculated that the increased peripheral NLR derived from increased NLR in the bone marrow. Moreover, the KEGG pathway analysis of upregulated DEGs in BM-neutrophil_1 was mainly enriched in osteoclast differentiation, which suggested that BM-neutrophil_1 may be closely involved in the mechanisms of osteopenia. Furthermore, the fact that only Naïve_B was left in STZ-induced T1D mice and that the RD/RC of BM-neutrophil_1/Naïve_B was the highest both suggested that BM-neutrophil_1 and Naïve_B were key cell subsets responsible for the negative correlation between the NLR and BMD. In addition, there was also an increasing trend in the RD/RC of BM-neutrophil_1/DCs, monocytes/DCs, and monocytes/B lymphocytes, suggesting that DCs and monocytes may become diagnostic indicators for T1D and T1D-induced complications.

Inevitably, there were still few limitations in our studies. In addition to the STZ-induced T1D model, nonobese diabetic (NOD) mouse, BioBreeding/Worcester rat, and lymphocytic choriomeningitis virus-induced model could also represent T1D animal models [51]. We limited our model in this research to STZ-induced T1D mice only. This limitation may result in an incomplete representation of the T1D model, but the STZ-induced T1D model was chosen as it could provide a relatively better understanding of the pathogenesis of T1D and T1D-induced osteopenia. We also acknowledged that NOD mice had become the preferred model for preclinical studies of T1D [51]. Thus, a complementary single-cell RNA sequencing analysis of the bone marrow in NOD mice might provide another comprehensive view.

Conclusion

Overall, our data objectively revealed the profiles of bone marrow cells in STZ-induced T1D mice for the first time through single-cell RNA sequencing analysis. In particular, the proportions of immune cells were chosen to analyze further since most of the bone marrow cells were $CD45^+$ cells. The occurrence of osteopenia in STZ-induced T1D mice was also confirmed. Furthermore, through single-cell flow cytometry and correlation analyses, we found that the increased ratio of BM-neutrophil/B lymphocytes negatively correlates with osteopenia in STZ-induced T1D mice, which may reason for an increased peripheral NLR in blood. Meanwhile, GO and KEGG analyses showed that BM-neutrophils and B lymphocytes were involved in the pathogenesis of T1D and T1D-induced osteopenia. Thereafter, in-depth studies on BM-neutrophils and B lymphocytes may be conducted to enhance understanding of T1D and T1D-induced osteopenia mechanisms. Studies of such may suggest that precise regulation of immune cells in the bone marrow could potentially become a novel strategy for treating T1D and preventing T1D-induced osteopenia.

Compliance with Ethics Requirements

All Institutional and National Guidelines for the care and use of animals (fisheries) were followed.

Data availability

All relevant data are available from the authors upon request. The raw data files of ScRNA-seq have been deposited in the Gene Expression Omnibus with following association number: GSE182986.

Declaration of Competing Interest

The authors declare that they have no known competing financial interests or personal relationships that could have appeared to influence the work reported in this paper.

Acknowledgements

This study was supported in part by grants from the National Natural Science Foundation of China (NO. 81972138, NO. 81972075 and NO. 81572229). Thanks for the technical support provided by the core facilities, Zhejiang University School of Medicine, especially the flow cytometry assay provided by Yingying Huang, Jiajia Wang, and Yanwei Li. Thanks for the technical support provided by Key Laboratory of Bone and Soft Tissue Injury Repair of Shanxi Province. Thanks for the English language editing support provided by Tong Zuo from the University of Chicago, USA.

Appendix A. Supplementary material

Supplementary data to this article can be found online at https://doi.org/10.1016/j.jare.2022.01.006.

References

[1] Atkinson MA, Eisenbarth GS, Michels AW. Type 1 diabetes. Lancet 2014;383(9911):69–82.
[2] Barnett R. Type 1 diabetes. Lancet 2018;391(10117):195. doi: https://doi.org/10.1016/S0140-6736(18)30024-2.
[3] Green A, Hede SM, Patterson CC, Wild SH, Imperatore G, Roglic G, et al. Type 1 diabetes in 2017: global estimates of incident and prevalent cases in children and adults. Diabetologia 2021;64(12):2741–50.
[4] Huang J, Xiao Y, Xu A, Zhou Z. Neutrophils in type 1 diabetes. J Diabetes Investig 2016;7(5):652–63.
[5] Ayhan H, Kasapkara HA, Aslan AN, Durmaz T, Keleş T, Akçay M, et al. Relationship of neutrophil-to-lymphocyte ratio with aortic stiffness in type 1 diabetes mellitus. Can J Diabetes 2015;39(4):317–21.
[6] Weber DR, Schwartz G. Epidemiology of skeletal health in type 1 diabetes. Curr Osteoporos Rep 2016;14(6):327–36.
[7] Wang JF, Lee MS, Tsai TL, et al. Bone morphogenetic protein-6 attenuates type 1 diabetes mellitus-associated bone loss. Stem Cells Transl Med 2019;8(6):522–34.
[8] Hu Y, Li X, Yan X, Huang G, Dai R, Zhou Z. Bone mineral density spectrum in individuals with type 1 diabetes, latent autoimmune diabetes in adults, and type 2 diabetes. Diabetes Metab Res Rev. 2021;37(3).
[9] Mollinedo F. Neutrophil degranulation, plasticity, and cancer metastasis. Trends Immunol 2019;40(3):228–42.
[10] Park J, Park J, Shin J-H, Oh Y-L, Jung H-A, Chung M-K, et al. Prognostic value of the neutrophil-to-lymphocyte ratio before and after radiotherapy for anaplastic thyroid carcinoma. Cancers (Basel) 2021;13(8):1913. doi: https://doi.org/10.3390/cancers13081913.
[11] Sánchez-Canteli M, Juesas L, Redin E, Calvo A, López F, Astudillo A, et al. Immune cell infiltrates and neutrophil-to-lymphocyte ratio in relation to response to chemotherapy and prognosis in laryngeal and hypopharyngeal squamous cell carcinomas. Cancers (Basel) 2021;13(9):2079. doi: https://doi.org/10.3390/cancers13092079.
[12] Feng Z, Yu Q, Yao S, Luo L, Zhou W, Mao X, et al. Early prediction of disease progression in COVID-19 pneumonia patients with chest CT and clinical characteristics. Nat Commun 2020;11(1). doi: https://doi.org/10.1038/s41467-020-18786-x.
[13] Dong C-H, Wang Z-M, Chen S-Y. Neutrophil to lymphocyte ratio predict mortality and major adverse cardiac events in acute coronary syndrome: a systematic review and meta-analysis. Clin Biochem 2018;52:131–6.
[14] Liu W, Huang Z, Tang S, Wei S, Zhang Z. An evaluation of homocysteine, C-reactive protein, lipid levels, neutrophils to lymphocyte ratio in postmenopausal osteopenic women. Gynecol Endocrinol 2016;32(6):446–8.
[15] Palmacci F, Toti E, Raguzzini A, Catasta G, Aiello P, Peluso I, et al. Neutrophil-to-lymphocyte ratio, mediterranean diet, and bone health in coeliac disease patients: a pilot study. Oxid Med Cell Longev 2019;2019:1–14.

[16] Caputa G, Castoldi A, Pearce EJ. Metabolic adaptations of tissue-resident immune cells. Nat Immunol 2019;20(7):793–801.
[17] Tuominen JT, Impivaara O, Puukka P, Rönnemaa T. Bone mineral density in patients with type 1 and type 2 diabetes. Diabetes Care 1999;22(7):1196–200.
[18] Strotmeyer ES, Cauley JA, Orchard TJ, Steenkiste AR, Dorman JS. Middle-aged premenopausal women with type 1 diabetes have lower bone mineral density and calcaneal quantitative ultrasound than nondiabetic women. Diabetes Care 2006;29(2):306–11.
[19] Like AA, Rossini AA. Streptozotocin-induced pancreatic insulitis: new model of diabetes mellitus. Science 1976;193(4251):415–7.
[20] Kang X, Li C, Xie Y, He L-L, Xiao F, Zhan K-B, et al. Hippocampal ornithine decarboxylase/spermidine pathway mediates H(2)S-alleviated cognitive impairment in diabetic rats: involving enhancment of hippocampal autophagic flux. J Adv Res 2021;27:31–40.
[21] Song L, Yuan J, Liu Y, et al. Ghrelin system is involved in improvements in glucose metabolism mediated by hyperbaric oxygen treatment in a streptozotocin-induced type 1 diabetes mouse model. Mol Med Rep 2020;22(5):3767–76.
[22] Hohlbaum K, Bert B, Dietze S, Palme R, Fink H, Thöne-Reineke C, et al. Severity classification of repeated isoflurane anesthesia in C57BL/6JRj mice-Assessing the degree of distress. PLoS ONE 2017;12(6):e0179588. doi: https://doi.org/10.1371/journal.pone.0179588.
[23] Zhu J, Siclari VA, Qin L. Isolating endosteal mesenchymal progenitors from rodent long bones. Methods Mol Biol 2015;1226:19–29.
[24] Dura B, Choi JY, Zhang K, et al. scFTD-seq: freeze-thaw lysis based, portable approach toward highly distributed single-cell 3' mRNA profiling. Nucleic Acids Res 2019;47(3).
[25] Liao Y, Smyth GK, Shi W. featureCounts: an efficient general purpose program for assigning sequence reads to genomic features. Bioinformatics 2014;30(7):923–30.
[26] Satija R, Farrell JA, Gennert D, Schier AF, Regev A. Spatial reconstruction of single-cell gene expression data. Nat Biotechnol 2015;33(5):495–502.
[27] Butler A, Hoffman P, Smibert P, Papalexi E, Satija R. Integrating single-cell transcriptomic data across different conditions, technologies, and species. Nat Biotechnol 2018;36(5):411–20.
[28] Yu G, Wang L-G, Han Y, He Q-Y. clusterProfiler: an R package for comparing biological themes among gene clusters. OMICS 2012;16(5):284–7.
[29] Che X, Chen T, Wei L, Gu X, Gao Y, Liang S, et al. MicroRNA-1 regulates the development of osteoarthritis in a Col2a1-Cre-ERT2/GFPfl/fl-RFP-miR-1 mouse model of osteoarthritis through the downregulation of Indian hedgehog expression. Int J Mol Med 2020;46(1):360–70.
[30] Liu C, Zhang H, Tang X, Feng R, Yao G, Chen W, et al. Mesenchymal stem cells promote the osteogenesis in collagen-induced arthritic mice through the inhibition of TNF-α. Stem Cells Int 2018;2018:1–10.
[31] Golda M, Mótyán JA, Nagy K, Matúz K, Nagy T, Tőzsér J. Biochemical characterization of human retroviral-like aspartic protease 1 (ASPRV1). Biomolecules 2020;10(7):1004. doi: https://doi.org/10.3390/biom10071004.
[32] Miyake Y, Toyonaga K, Mori D, Kakuta S, Hoshino Y, Oyamada A, et al. C-type lectin MCL is an FcRγ-coupled receptor that mediates the adjuvanticity of mycobacterial cord factor. Immunity 2013;38(5):1050–62.
[33] Zheng Y, Zhang W, Ye Q, Zhou Y, Xiong W, He W, et al. Inhibition of Epstein-Barr virus infection by lactoferrin. J Innate Immun 2012;4(4):387–98.
[34] Chen Z, Wang L. The clinical significance of UBE2C gene in progression of renal cell carcinoma. Eur J Histochem 2021;65(2).
[35] Gómez Hernández G, Morell M, Alarcón-Riquelme ME. The role of BANK1 in B cell signaling and disease. Cells 2021;10(5):1184. doi: https://doi.org/10.3390/cells10051184.
[36] Wong KY, Baron R, Seldon TA, Jones ML, Rice AM, Munster DJ. CD83 antibody inhibits human B cell responses to antigen as well as dendritic cell-mediated CD4 T cell responses. J Immunol 2018;200(10):3383–96.
[37] Agathangelidis A, Chatzidimitriou A, Gemenetzi K, et al. Higher-order connections between stereotyped subsets: implications for improved patient classification in CLL. Blood 2021;137(10):1365–76.
[38] Edner NM, Heuts F, Thomas N, Wang CJ, Petersone L, Kenefeck R, et al. Follicular helper T cell profiles predict response to costimulation blockade in type 1 diabetes. Nat Immunol 2020;21(10):1244–55.
[39] Chiou J, Geusz RJ, Okino M-L, Han JY, Miller M, Melton R, et al. Interpreting type 1 diabetes risk with genetics and single-cell epigenomics. Nature 2021;594(7863):398–402.
[40] Valderrábano RJ, Lui L-Y, Lee J, Cummings SR, Orwoll ES, Hoffman AR, et al. Bone density loss is associated with blood cell counts. J Bone Miner Res 2017;32(2):212–20.
[41] Huang W, Wu J, Yang H, Xiong Y, Jiang R, Cui T, et al. Milk fat globule-EGF factor 8 suppresses the aberrant immune response of systemic lupus erythematosus-derived neutrophils and associated tissue damage. Cell Death Differ 2017;24(2):263–75.
[42] Heestermans M, Salloum-Asfar S, Streef T, Laghmani EH, Salvatori D, Luken BM, et al. Mouse venous thrombosis upon silencing of anticoagulants depends on tissue factor and platelets, not FXII or neutrophils. Blood 2019;133(19):2090–9.
[43] Deng C, Xiang Y, Tan T, Ren Z, Cao C, Huang G, et al. Altered peripheral B-lymphocyte subsets in type 1 diabetes and latent autoimmune diabetes in adults. Diabetes Care 2016;39(3):434–40.
[44] Maahs DM, West NA, Lawrence JM, Mayer-Davis EJ. Epidemiology of type 1 diabetes. Endocrinol Metab Clin North Am 2010;39(3):481–97.
[45] Valle A, Giamporcaro GM, Scavini M, Stabilini A, Grogan P, Bianconi E, et al. Reduction of circulating neutrophils precedes and accompanies type 1 diabetes. Diabetes 2013;62(6):2072–7.
[46] Qin J, Fu S, Speake C, Greenbaum CJ, Odegard JM. NETosis-associated serum biomarkers are reduced in type 1 diabetes in association with neutrophil count. Clin Exp Immunol 2016;184(3):318–22.
[47] Salami F, Lee HS, Freyhult E, Elding Larsson H, Lernmark Å, Törn C. Reduction in white blood cell, neutrophil, and red blood cell counts related to sex, HLA, and islet autoantibodies in swedish TEDDY children at increased risk for type 1 diabetes. Diabetes 2018;67(11):2329–36.
[48] Huang J, Xiao Y, Zheng P, Zhou W, Wang Y, Huang G, et al. Distinct neutrophil counts and functions in newly diagnosed type 1 diabetes, latent autoimmune diabetes in adults, and type 2 diabetes. Diabetes Metab Res Rev 2019;35(1):e3064. doi: https://doi.org/10.1002/dmrr.v35.110.1002/dmrr.3064.
[49] Diana J, Simoni Y, Furio L, Beaudoin L, Agerberth B, Barrat F, et al. Crosstalk between neutrophils, B-1a cells and plasmacytoid dendritic cells initiates autoimmune diabetes. Nat Med 2013;19(1):65–73.
[50] Pais Ferreira D, Silva JG, Wyss T, Fuertes Marraco SA, Scarpellino L, Charmoy M, et al. Central memory CD8(+) T cells derive from stem-like Tcf7(hi) effector cells in the absence of cytotoxic differentiation. Immunity 2020;53(5):985–1000.e11.
[51] Reed JC, Herold KC. Thinking bedside at the bench: the NOD mouse model of T1DM. Nat Rev Endocrinol 2015;11(5):308–14.